3

Egypt. J. Phys. **Vol. 51,** pp. 35-56 (2023)

Egyptian Journal of Physics

Zn1-xMgxO Nanocomposites: Synthesis, Structural, Optical Propertiesand Antibacterial Activity

Samah Taha[1], Mohammed Ezzeldien[2], K. H. Omran[1, 3], M. S. Abd El-sadek[*1]

[1]*Nanomaterials Lab., Physics Department, Faculty of Science, South Valley University, Qena-83523, Egypt.*
[2]*Mechanical Lab, Physics Department, Faculty of Science, South Valley University, Qena-83523, Egypt.*
[3]*Laser Tech. & Environment Lab., Physics Department, Faculty of Science, South Valley University, Qena 83523, Egypt.*

Abstract

Zn1-xMgxO nanocomposites were synthesized by a modified sol-gel method. The effect of increasing Mg content on structural, optical properties, and antibacterial activity was studied. The structure and physical properties of the Zn1-xMgxO nanocomposites were characterized by thermogravimetric (TG) analysis, Fourier-transform infrared spectroscopy (FT-IR), X-Ray Diffraction (XRD), and transmission electron microscope (TEM). The optical properties were investigated by UV-visible spectroscopy and Photo luminesce spectra (PL). The thermal properties and the weight stability were studied for the samples using TG-Analysis to determine the best annealing temperature at 550 °C. The XRD result confirms that clear indications for segregation into a hexagonal and a cubic phase are found for samples having magnesium content between 0.2 $\square$ x $\square$ 0.8. According to Scherer's formula, the average particle size of the synthesized nanocomposites is in the range of 16.32- 25.56 nm. TEM images showed hexagonal, irregular, and spherical shapes. The calculated band gap energies (Eg) of the Zn1-xMgxO nanocomposites were changed from 3.18 to 3.31 eV by increasing Mg concentration in the Zn1-xMgxO nanocomposites. The XRD and UV-vis analysis results indicated that the physical characteristics of Zn1-xMgxO nanocomposites were dependent on increasing the incorporation of Mg2+ ion concentration. The antibacterial assessment illustrated that the ZnO-MgO nanocomposites showed excellent antibacterial activity, the inhibition zoon increases from 12 mm for pure ZnO to 15 mm for Zn1-xMgxO nanocomposites with Mg ratio (x=0.4). The result concluded that Zn1-xMgxO nanocomposites have significant potential for antibacterial applications.

Keywords: Zn1-xMgxOnanocomposites, Structural analysis, Optical Properties, Antibacterial activity.

1. Introduction

Metal oxide semiconductors have a great potential in practical applications such as sensors, batteries, optoelectronics, solar cells, catalysis, and biomedicals[1], [2]. Nanocrystalline zinc oxide (ZnO), an n-type metal oxide semiconductor, is one of the metal oxides which comprises wide band gap energy of 3.37 eV, large excitation binding energy of 60 meV in addition good optical and electrical responses. ZnO has a lot of important applications in the field of solar cell, optoelectronics, light emitting devices, medical sectors, waste remediation and catalysis.Tuning of excitation wavelength of this semiconductor is essential totune its optical, electrical, and magnetic properties which play important roles during practical applications [3].Metal oxide nanoparticles (NPs) exhibit many functional characteristics and have a wide range of applications such as optoelectronics, sensors, photocatalyst, and antibacterial applications[4]. As a result, it was necessary to create sources of active antibacterial nanomaterials due to increased antibiotic resistance [5]. Mixing or doping of one metal oxide semiconductor with other helps in tuning of this properties. As the doping of ZnO with magnesium (bandgap of 7.3 eV) can increase the UV luminescence intensity by adjusting its wavelength [6]. (Zn1-xMgxO)

_____

nanocomposites display improved optical properties which enhances the bandgap due to the different crystallites and electronic coupling between ZnO and MgO. Several synthesis techniques were used to synthesis (Zn1-xMgxO) nanocompositessuch as hydrothermal growth [7], sonochemical [8], thermal evaporation techniques[9], sol gel technique [4], high pressure synthesis [10]and microwave assisted methods [11]. Sol-gel is a simple, cost-effective,and eco-friendly method to synthesis (Zn1-xMgxO) nanocomposites [12].In the present study, the synthesis of pure ZnO, pure MgO and Zn1-xMgxO nanocomposites was carried out by the sol–gel method and calcined at 550 °C for 2 hours. The effect of increasing Mg content on the physical properties and the antibacterial activity was studied. The synthesized nanocomposites were characterized by various characterization techniques.

2. Materials and Methods

2.1 Materials

Zinc acetate dihydrate, oxalic acid, Magnesium nitrate, Sodium hydroxide and ethanol (as a solvent) were used to prepare $Zn_{1-x}Mg_xO$ nanocomposites. All the preparation materials were obtained from Oxford Lab. Chem. (India) limited Co.

2.2 Preparation of Zn1-xMgxO nanoparticles

$Zn_{1-x}Mg_xO$ nanocomposites with various magnesiumcontent (x= 0, 0.2, 0.4, 0.5, 0.6, 0,8 and 1) were synthesized by adding various weights of magnesium nitrate dissolved in ethanol (20 mL) to the zinc acetate-oxalic acid solution while the solution was being stirred. Themixed solution was dried at 80°C for 12 hours. Finally, the dried powder was calcined at 550 °C for 2 hours.

2.3. Characterization

The crystal structures of pure ZnO, pure MgO, and $Zn_{1-x}Mg_xO$ nanocomposites were analyzed by (Philips, PW 1710) X-ray diffractometer with CuKα line (λ = 1.54183Å) in the range 2θ from 10° to 90°. The data derived from investigating XRD peaks of ZnO NPs were carried out to calculate the crystallite size and the lattice strain based on both Scherrer formula and Williamson–Hall model. The functional groups of tested samples were recorded by FTIR spectrum (JASCO FT-IR 4100) in the range of wavenumber between 4000 and 400 cm^{-1}. The morphology of the synthesized samples was carried out by a High-Resolution transmission Electron Microscope of type (Philips, EM-2100 PW 1710 Japan). JASCO 670 UV spectrophotometer was used to measure the UV–Vis'sabsorption spectrum of the samples in the range from 200 to 800 nm. A photoluminescence study was performed using a fluorescence spectrophotometer (JASCO 860j0) under an excitation wavelength of 320 nm.

2.4 Antibacterial activity

The ZnO and MgO NPs are studied extensively to explore their utility as potential antibacterial agents. Several factors such as less toxicity and heat resistance are accountable for the use of nanoparticles in biological applications. Zinc oxide and Mg^{2+} doped ZnO NPs are considered bio-safe substances but have impacts on biological organisms by their photo-oxidizing and photocatalytic ability[13]. Antibacterial activity of synthesized $Zn_{1-x}Mg_xO$ nanocomposites was tested by the Agar disk-diffusion method against pathogenic bacterial strains such as gram-negative (Escherichia coli (E. Coli)) and gram-positive bacteria (Enterococcus faecalis) to determine their ability as a potential antimicrobial agent. The nutrient medium was prepared by dissolving 28 g of nutrient agar medium in 1000 ml of distilled water, adjusting the pH to 7.3 (± 0.1), and subjecting the medium to sterilization in an autoclave at 121 °C for 20 min. To prepare nutrient agar plates, 20-25 ml of sterile nutrient agar medium was poured into Petri-dishes and allowed to solidify. Then, mature broth culture of individual pathogenic bacterial strains was spread all over the surface of agar plates using sterilized cotton swabs. The test samples were dissolved by ultrasound to make suspension with concentration (0.005 g of the sample to 1ml of distilled water). Then, filter paper discs (about 0.6 mm in diameter), containing the test samples at a desired concentration, are placed on the agar surface. The Petri dishes are incubated under suitable conditions at 37 °C for 24 hours. Antimicrobial agent diffuses into the agar, inhibits germination, growth of the test microorganism, and then the diameters of inhibition growth zones are measured. The experiments were carried out in duplicate with each compound and the average values were calculated to estimate the antibacterial activity.

The antibacterial activity of Metal oxides is primarily determined by three variables: the generation of reactive oxygen species (ROS), the release of Zn^{2+} ions for the ZnO system, and the reduction of grain size by Mg^{2+}doped ZnO nanoparticles. These variables increased surface interaction, surface tension, and electromotive forces. When ROS generation is a more powerful oxidizing agent and directly penetrates the cell membrane of the bacteria, it causes injuries and prevents cell growth, whereas negatively charged hydroxyl radicals and superoxide anions cannot penetrate the cell membrane but cause severe damage to proteins, and profiles of the bacteria's outer wall, resulting in the bacteria's destruction [14]. These reasons explain why the antibacterial

_____

..

activity of the ZnO nanoparticles andZn$_{1-x}$Mg$_x$O nanocomposites could be enhanced by increasing the Mgcontent.

3. Results and Discussion

3.1 Physical Properties of (Zn1-xMgxO) nanocomposites
Thermal analysis spectra of Zn$_{1-x}$Mg$_x$O nanocomposite

Thermal analysis of Zn$_{1-x}$Mg$_x$O nanocomposites (0 ≤ x ≤ 1) was investigated by thermogravimetric analysis (TG) and differential scanning calorimetry (DSC). The thermal stability and the heat treatment of samples were determined by experiments at a heating rate of 10 °C/min from room temperature to 800 °C. TG curve in Figure (1) shows four weight loss regions: Region (1) from room temperature to 120 °C shows the weight loss around 3% up to 10%, which is resulted due to the evaporation of surface adsorbed water. Region (2) from 120 °C to 290 °C shows a weight loss around 9% up to 30% which was related to the combustion of organic materials. Region (3) from 290 °C to 490 °C shows a drastic weight loss around 19% up to 66%, it was related to the crystallization of Zn$_{1-x}$Mg$_x$O nanoparticles [15]. Region (4), at the temperature range above 500 °C, the weight was approximately constant, and the samples are more thermally stable, which indicates the formation of Zn$_{1-x}$Mg$_x$O nanoparticles at different values of Mg content x. So, the calcinated temperature for the Zn$_{1-x}$Mg$_x$O nanoparticles was chosen at 550 °C[16]. The DSC curve shows that all the samples have two major endothermic peaks as seen in Figure (2). The first one is the broad endothermic peak approximately around (100 °C – 200 °C) corresponds to the removal of residual water and solvent. The second endothermic peaks approximately appear around (300 – 500 °C) were attributed to the decomposition reaction of precipitates to get Zn$_{1-x}$Mg$_x$O nanoparticles. Only the Zn$_{0.6}$Mg$_{0.4}$O sample shows an exothermic peak approximately around 350 °C attributed to the volatile organic moieties produced by the dissociation of precursor to react with O$_2$ to form CO$_2$ and H$_2$O [17].
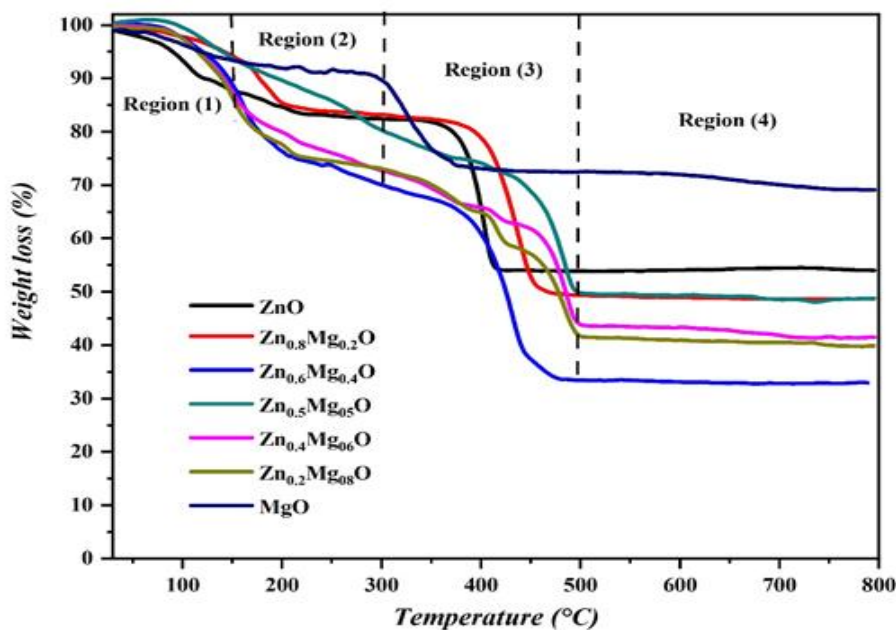

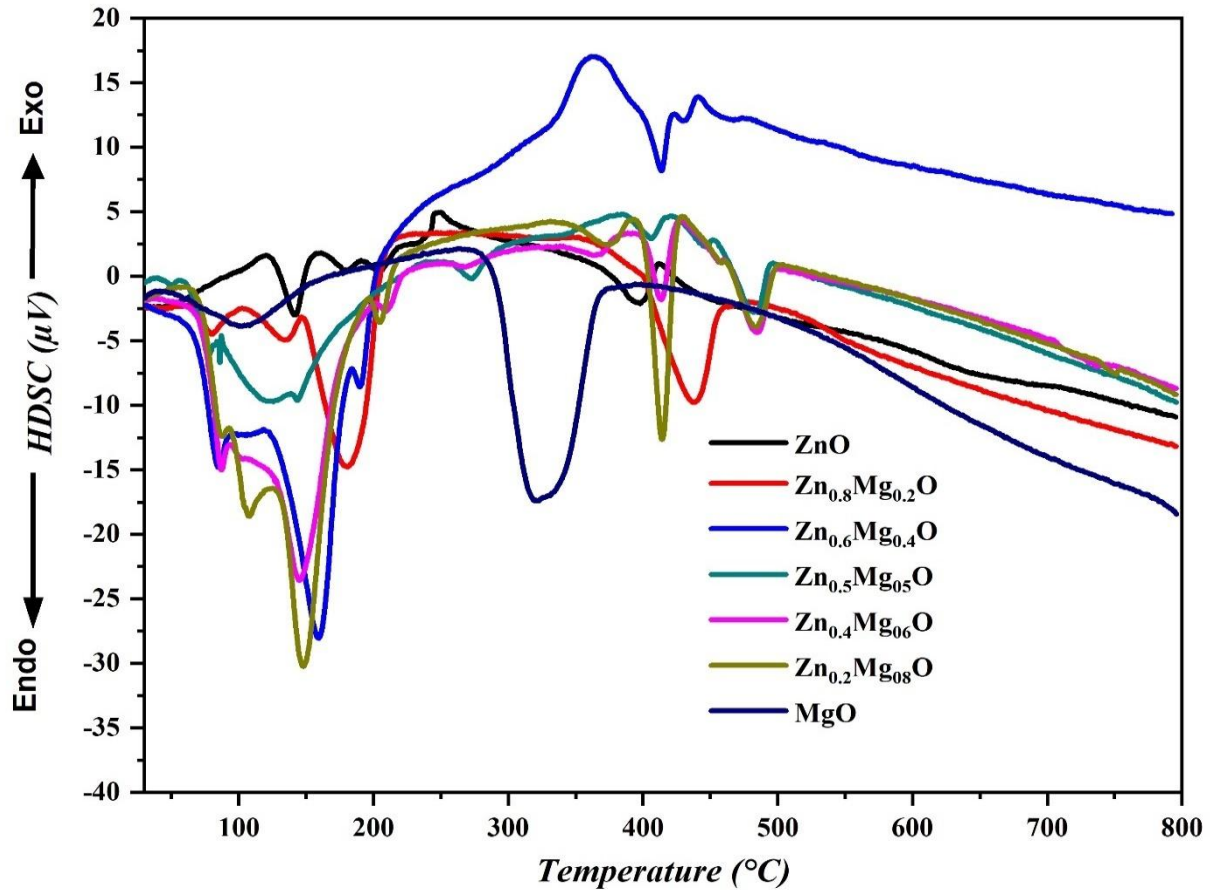**Fig. 1. Thermal analysis spectra of Zn1-xMgxO nanocomposites (0 ≤ x ≤ 1).**

_____

_____

Fig. 2. Comparison The differential scanning calorimetry (DSC) spectra of Zn1-xMgxO nanocomposites.

FTIR Analysis

Figure 3 shows FTIR transmittance analysis of $Zn_{1-x}Mg_xO$ nanocomposites. The spectrum indicates a broad peak around the 3450 cm^{-1} due to the primary O–H functional group which is the main absorption point of metal ions changed [6]. The peak appeared around 1450 cm^{-1} may be due to the presence of bending vibration of the O-H bond which is associated with the absorbed water surface from the synthesized $Zn_{1-x}Mg_xO$ nanoparticles. It is noticed that peak intensity increases with increasing the ratio of MgO, it is well known that MgO is a highly absorber material of H_2O and CO_2 molecules when exposed to the atmosphere [18]. The peak appeared at 870 cm^{-1} and around 500 cm^{-1} are due to Mg–O and Zn–O bonds, respectively, which confirms the formation of a pure nanocomposite form of synthesized metal oxides.
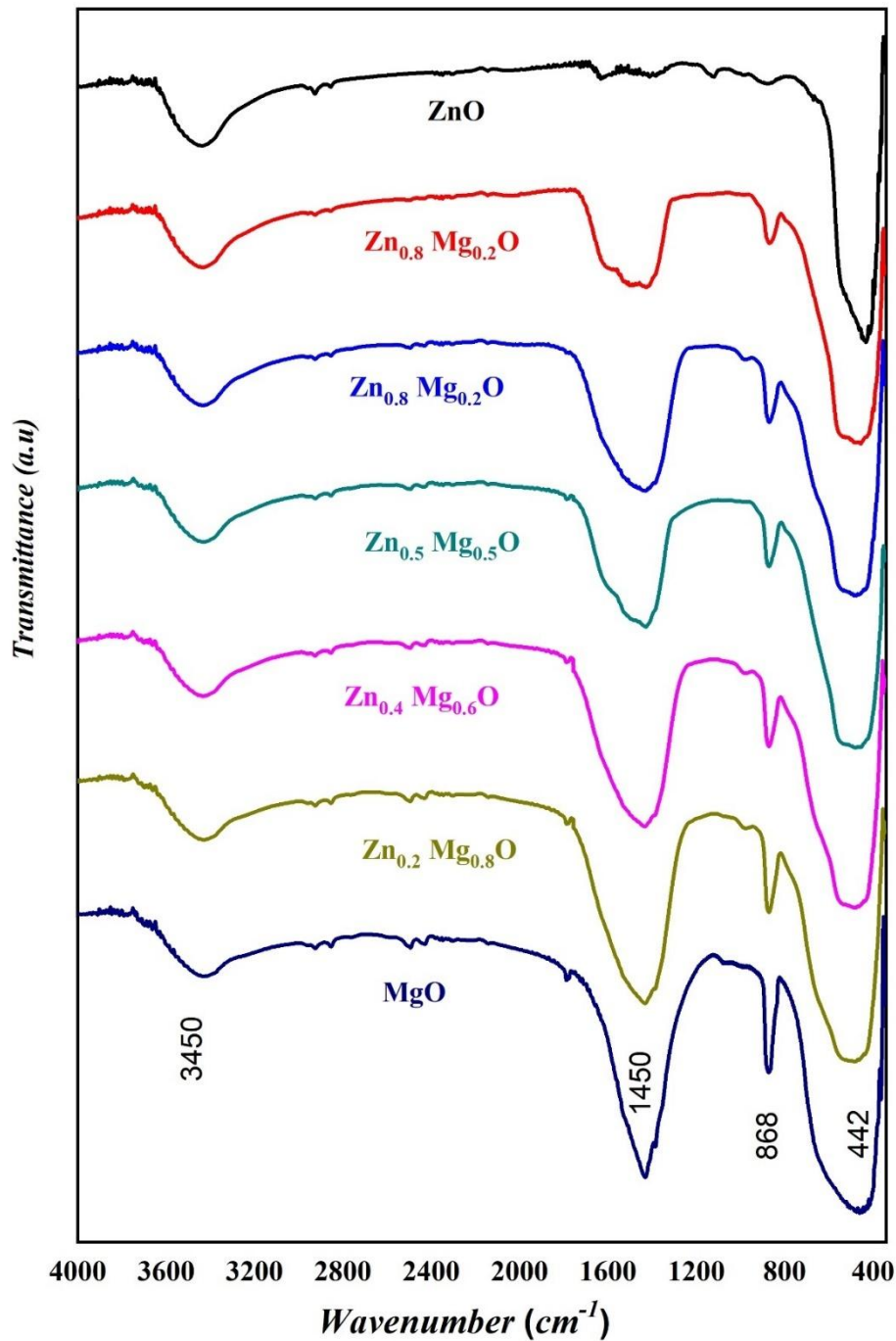
_____

..

Fig. 3. FTIR analysis of Zn1-xMgxO nanocomposites.

Structural and morphological properties of the $Zn_{1-x}Mg_xO$ nanoparticles

XRD and particle size analysis

Figure (4) shows the XRD patterns of pure ZnO, pure MgO, and the $Zn_{1-x}Mg_xO$ nanocomposites synthesized using sol-gel method. For pure ZnO NPs, hexagonal wurtzite phase is detected for all the observed peaks [JCPDS card no. 01-080-0075]. The polycrystalline ZnO nanoparticles are grown along the planes (100), (002), (101), (102), (110), (103), (201), (200), (112), (004), and (202) with the highest intensity corresponding to the (101) diffraction line. The XRD pattern of pure MgO NPs has a cubic phase well matched with the standard card (JCPDS no.01-079-0612). For the $Zn_{1-x}Mg_xO$ nanocomposites, all the diffraction peaks except three are well fitted with the JCPDS card 01-080-0075 and hence identified as hexagonal wurtzite structure of ZnO. The three unmatched diffraction peaks observed at $2\theta = 42.7$, 62.32, and 78.6^o are associated with the (hkl) planes (200),

_____

_____

(220), and (222) of cubic structured MgO (JCPDS card no. 01-079-0612) indicating the presence of the secondary phase of MgO, so, the samples have two mixed phases hexagonal phase of ZnO and cubic phase of MgO.

The results confirm that as the Mg concentration increases, the number of MgO peaks in the XRD pattern increase, and the cubic phase clearly appears in the nanocomposite samples. Even though the intensities of the peaks are remarkably affected by increasing of Mg concentration, the intensities of the secondary peaks were found to increase while the quality of ZnO peaks decrease with the increase in the Mg level.

The XRD behaviour gives a clear indication of segregation into a hexagonal and a cubic phase for samples with magnesium contents ranging from $0.2 \leq x \leq 0.8$. the sample of (x=0.2) showed a weak (200) reflection of the MgO phase, indicating that most of the material was in the form of ZnO hexagonal structure this is attributed to the hexagonal structure is more stable than the cubic structure because it has a lower total energy at x < 0.5. According to literature, the MgO segregation from the ZnO phase, in particular, occurs at lower x values [19]. Furthermore, at x values around 0.5, the $Zn_{1-x}Mg_xO$ nanocomposites typically grow with a mixed phase lattice structure [20].

The crystallite size of ZnO, MgO,and $Zn_{1-x}Mg_xO$ nanocomposites can be calculated from XRD pattern analysis by using Scherrer'sformula [21]:

$$\beta = K\lambda/D\cos\theta \qquad (1)$$

Where K is the shape factor (0.9), λ is the wavelength of Cu-Kα radiation (0.15406 nm), β is the peak width at half maximum in radians and θ is the Bragg's diffraction angle [22].

The lattice strain can be calculated using the Williamson- Hall (W–H) models [23],by plotting $4\sin\theta$ along the x-axis and $\beta\cos\theta$ along the y-axis as shown in Figure (5), where the slopeof fitting line gives the strain value, and the intercept (K λ /D) gives the crystal size. The results are summarized in Table (1).

$$\beta\cos\theta = (k\ \lambda/D) + 4\varepsilon\sin\theta \quad (2)$$

In the case of pure ZnO sample, the size of crystallite was (18.45 nm). The size of the crystallite decreases to (16.32 nm) with the increases in the Mg doping level up to (x=0.4) and for further increase in Mg doping level up to (x=0.5), the crystal size increases to (25.56 nm),after that the crystal size starts to decrease with increasing of Mg level up to (x=0.8). This obtained result can be interpreted based on the Zener pinning effect [24]. The Zener pinning effect refers to the restriction in the growth of crystallites and grain size caused by the crystal defects like vacancies and interstitials [25]. The Zener pinning effect states that the outward movement (expansion) of grain boundaries is limited by the retarding force generated by crystal imperfections such as vacancies and interstitials. In the present study, when Mg is doped with ZnO, the number of oxygen vacancies present in the ZnO lattice may be large. These oxygen vacancies restrict the growth of the crystallites. But, when the Mg doping level `increases, the incorporated Mg ions may fill these oxygen vacancies. As a result, the influence of retarding force decreases gradually, allowing the crystallites to grow larger in size. This trend is found to continue only up to Mg doping level (x=0.5) and then the excess Mg ions in the lattice are positioned as interstitials, which may again enhance the retarding force causing the crystallite size to decrease [26].
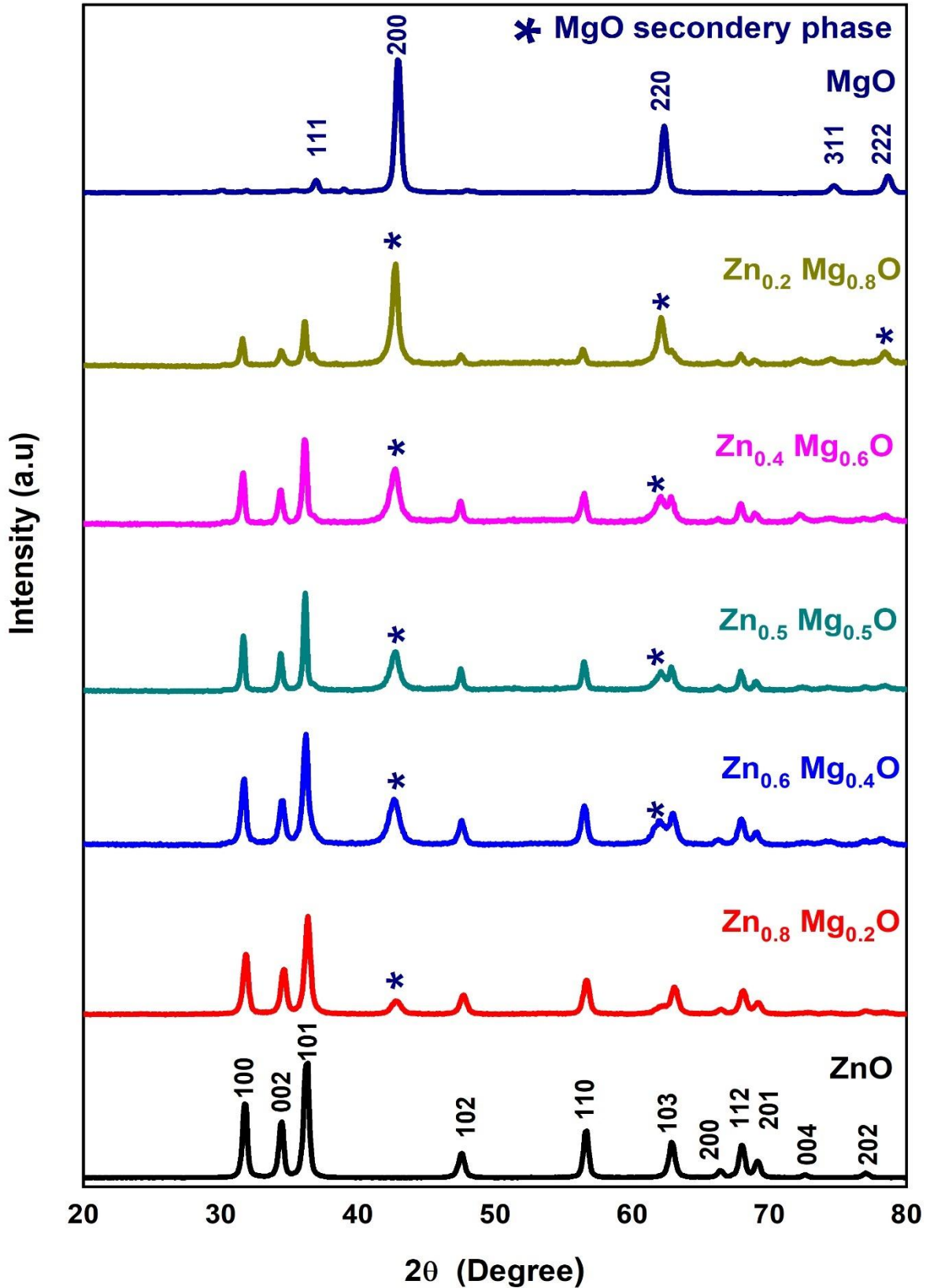
_____

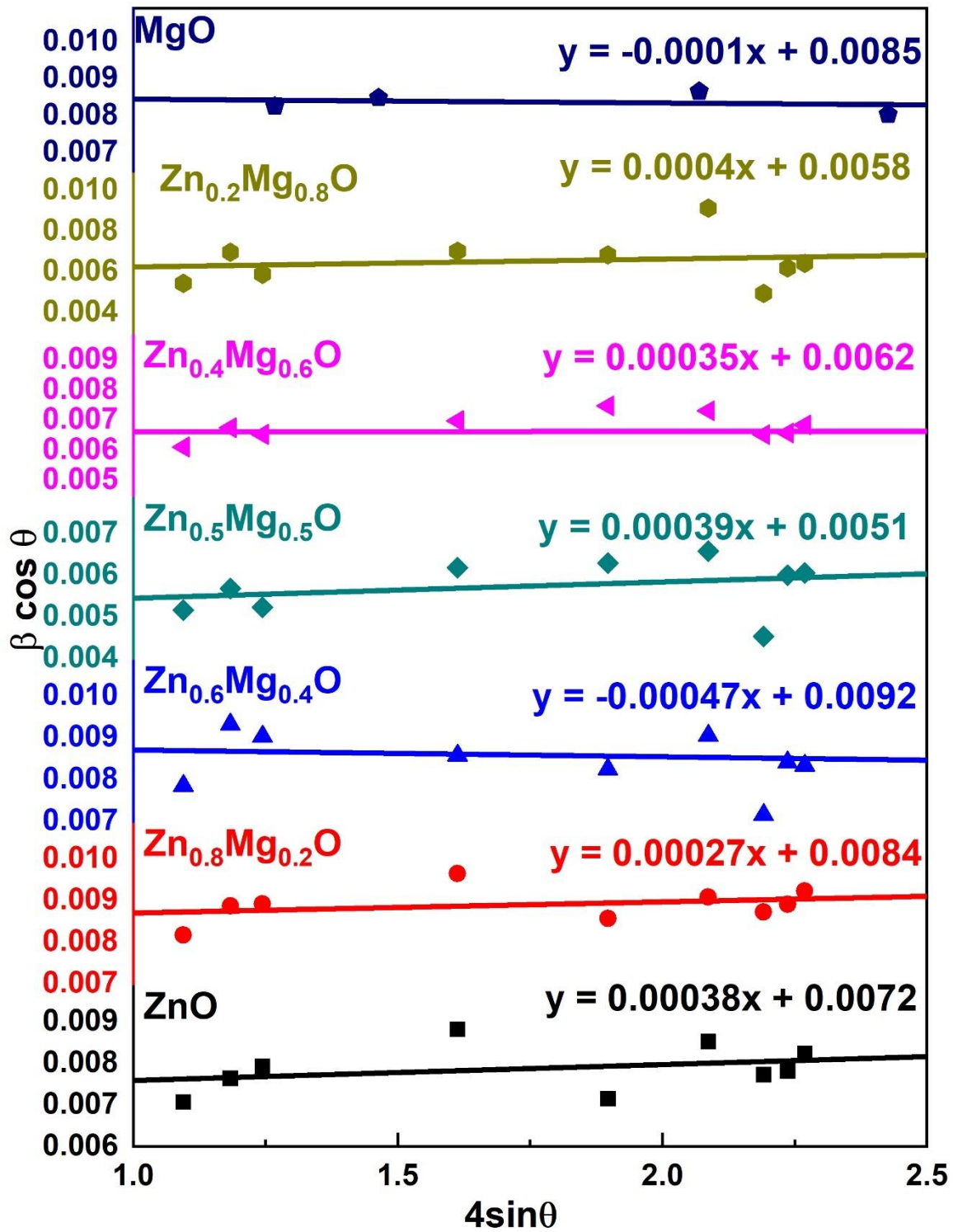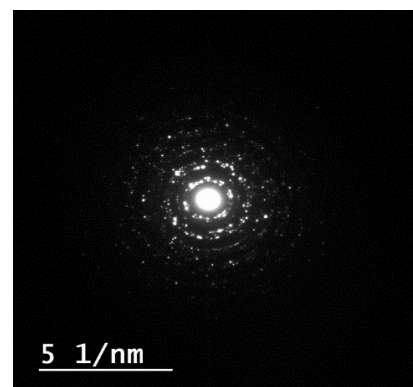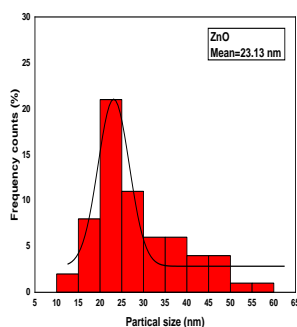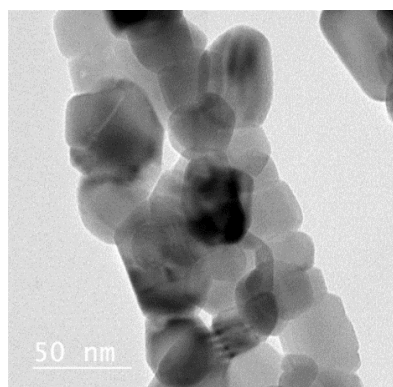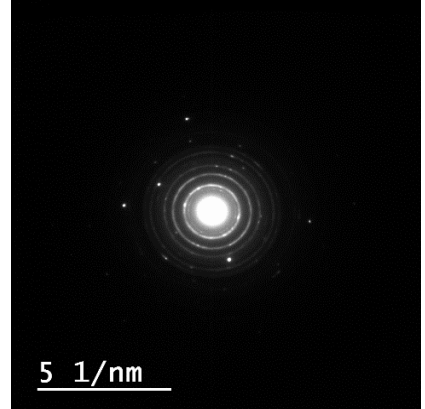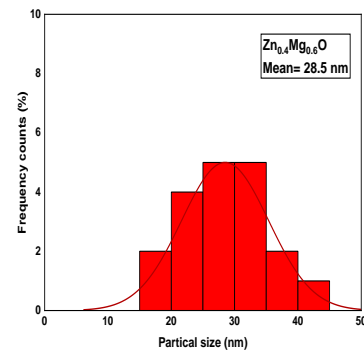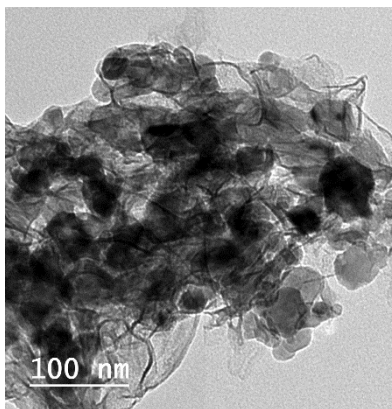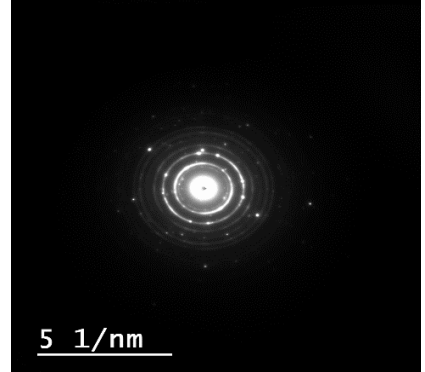**Fig 4. The XRD patterns of Zn1-xMgxO nanocomposites.**

Fig 5. The W–H plots of Zn1-xMgxO nanocomposites.

TABLE 1. The calculated crystal size, lattice strain, and energy gapof the $Zn_{1-x}Mg_xO$ nanocomposites.

Sample	Phase	Crystallite size (nm)		Strain	Eg (eV)
		Scherrer	W-H	$\varepsilon * 10^{-4}$	
ZnO	Wurtzite	18.49	20.10	3.8	3.18
$Zn_{0.8}Mg_{0.2}O$	Wurtzite/cubic	16.32	17.19	2.7	3.28
$Zn_{0.6}Mg_{0.4}O$	Wurtzite/cubic	17.29	15.75	4.7	3.30
$Zn_{0.5}Mg_{0.5}O$	Wurtzite/cubic	25.56	28.70	3.9	3.31
$Zn_{0.4}Mg_{0.6}O$	Wurtzite/cubic	22.15	23.37	3.5	3.32
$Zn_{0.2}Mg_{0.8}O$	Wurtzite/cubic	22.80	24.86	4.0	3.28
MgO	Cubic	17.38	16.95	1.0	5.22

TEM analysis for the ($Zn_{1-x}Mg_xO$) nanoparticles

The TEM measurement technique is a practical and appropriate method for analyzing the morphology of nanoparticles [27]. Figure (6) illustrates the morphological characteristics of $Zn_{1-x}Mg_xO$ nanoparticles. The images indicated hexagonal, irregular, and spherical shapes respectively. Crystal defects such as dislocations and stacking faults were discovered in other images. The particle sizes of $Zn_{1-x}Mg_xO$ nanocompositeswere found to be ranging from 23 to 75 nm. Figure (6) display histograms of particle size distribution of the NPs. These histograms indicate that the mean particle sizes of the ($Zn_{1-x}Mg_xO$) (X = 0, 0.2, 0.4, 0.5, 0.6, 0.8, 1) are approximately 23, 20, 21, 31, 28, 32, and 25 nm, respectively. The selected area diffraction (SAED) pattern clearly showed highly crystalline nature of $Zn_{1-x}Mg_xO$ nanocomposites.The results indicated that the crystallite size determined by Scherrer equation is smaller than crystallite size determined from Williamson–Hall method which is comparable to the particle size determined by TEM. This may be due to the fact that the Scherrer method actually measures the coherence length of the X-rays, any crystal imperfections will cause the calculated size to be smaller than the true size whereas the W-H method takes the macrostrain effect into consideration [28], [29], [30]. The TEM technique measures particle size, whereas the XRD technique only measures crystallite size, which is different from particle size. Because one particle can be made up of several crystallites, the particle size measured by TEM always be larger than the crystallite size measured by XRD.
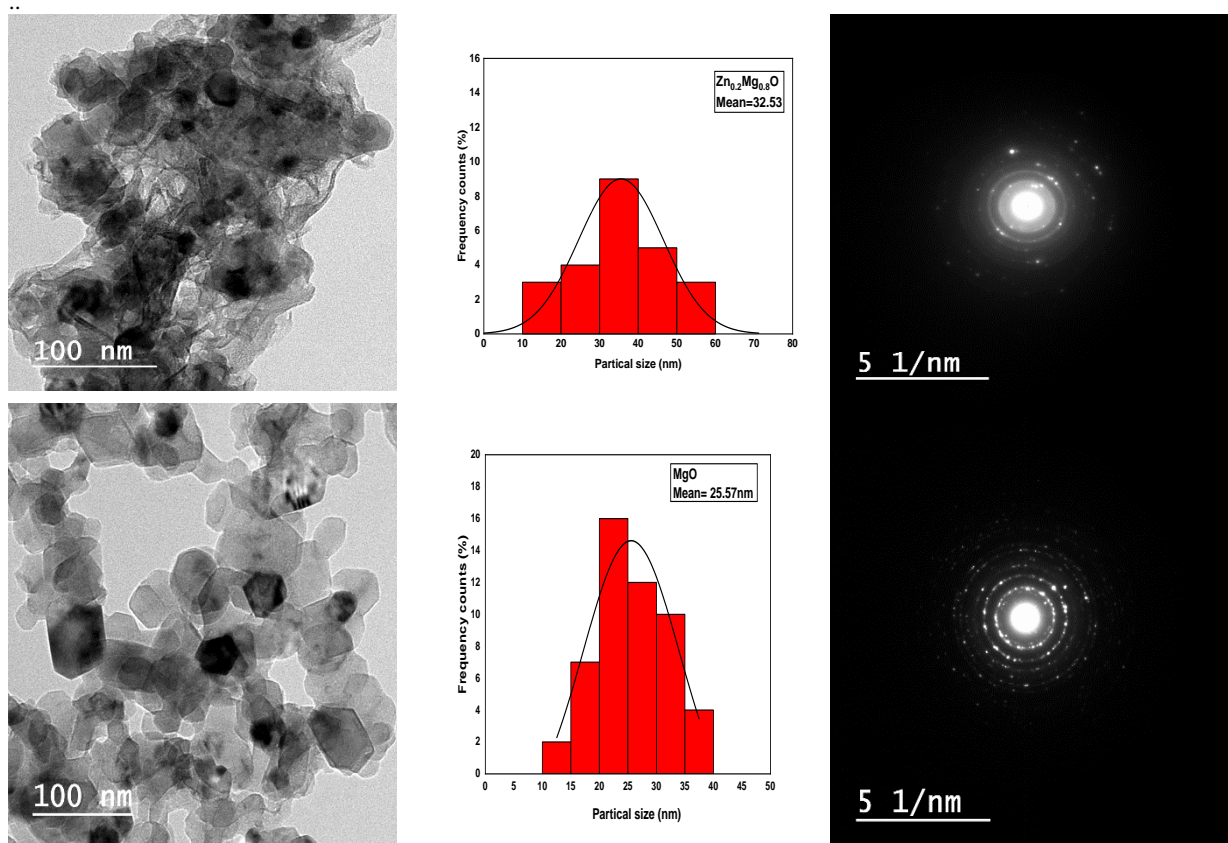
_____
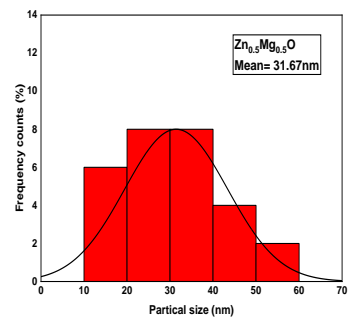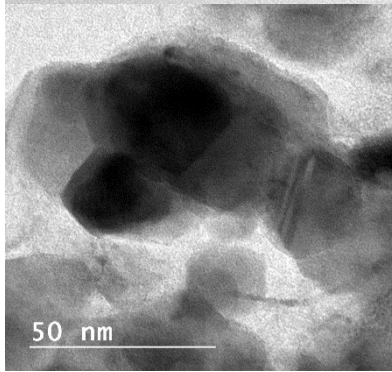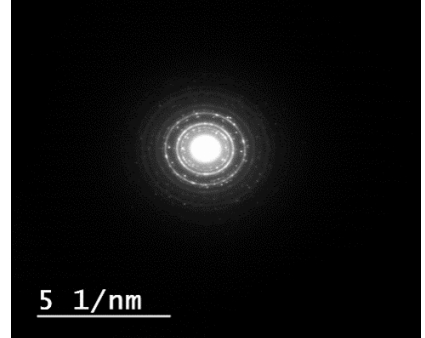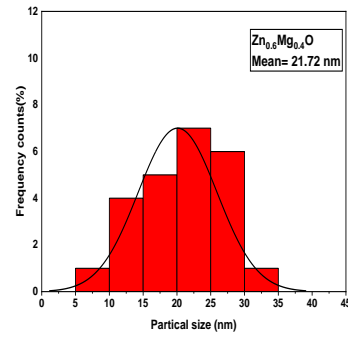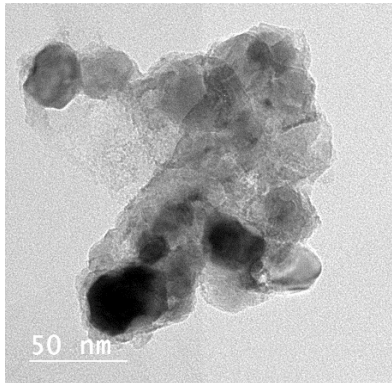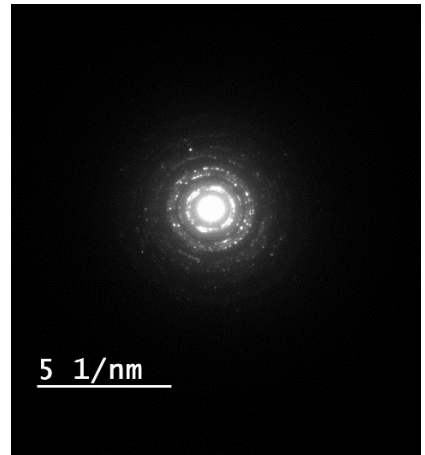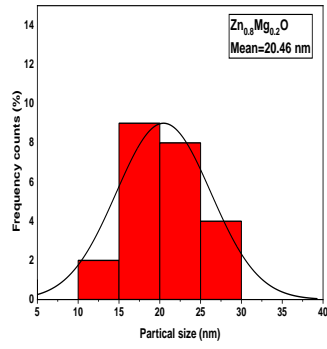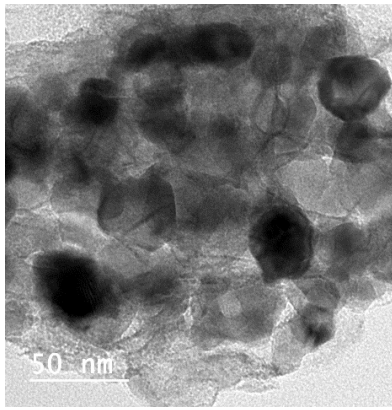
Fig. 6. (a) TEM image Zn$_{1-x}$Mg$_x$O nanocomposites, (b) the distribution of particles size, and (c) SAED pattern.

Optical properties of Zn$_{1-x}$Mg$_x$O nanoparticles
   (UV–vis) absorption spectroscopy

The optical properties of the ZnO-MgO NPs were determined from the absorption spectra in the wavelength range of 200–800 nm as presented in Figure (7). The results demonstrate that the incorporation of Mg^{2+} into the Zn^{2+} site of the wurtzite lattice parameters which appeared in the band edge shift to lower wavelength (blue shift). This absorption edge was blue shifted with the increase of Mg concentrations from 400 to 330 nm at the sample Zn$_{0.2}$Mg$_{0.8}$O, the reason of increasing the absorption might be due to defect in the grain sizes and oxygen deficiency [31]. Also this is due to the increase in surface roughness which leads to more absorption at the surface and so to less transparency and less reflectivity [32]. Figure (8) represents the optical transmittance spectra in the wavelength range of 200 ~ 800 nm at room temperature of the Zn$_{1-x}$Mg$_x$O nanoparticles. The Zn$_{1-x}$Mg$_x$O nanoparticles were highly transparent in the visible range with a sharp band edge absorption in the UV region. It was observed that transmittance is increased with the increase of the Mg^{2+} content in the Zn$_{1-x}$Mg$_x$O nanoparticles. It is observed that all the nanocomposite samples have high transmittance values in the visible range from 85 to 95%. In the UV range, it is noticed that the transmittance increased from 10 to 40 % as Mg content increased from x=0 to x =0.8 due to evidencing the substitution incorporation of Mg into the Zn site of the wurtzite lattice. This result verifies high optical quality of the Zn$_{1-x}$Mg$_x$O nanoparticles[12]. The UV absorption edge is directly linked to the optical band gap (Eg). The optical band gap is an important parameter for Mg-doped ZnO nanoparticles in various optical applications. The band gap can be estimated from the absorption edge by applying Tauc's relationship[12].The optical band (Eg) was estimated by assuming a direct transition (n is set equal to 1/2) between the valence and conduction bands[33]–[35]. As the transition in the ZnO is direct, Tauc equation become in the following form:

$$(\alpha h v)^2 = A\left(E_g - hv\right) \qquad (3)$$

_____

When A, α , hv are constant, absorption coefficient, and energy photon, respectively.The absorption coefficient α was calculated from the absorbance A by using the following equation:

$$\alpha = \frac{2.303 * A}{d} \quad (4)$$

Where d is the thickness of the sample pellet and equal to 0.05 cm.The optical band gap (Eg) of the $(Zn_{1-x}Mg_xO)$ nanoparticles was determined by plotting the experimentally observed values of $(\alpha h v)^2$ against (hv) as observed in Figure (9).The band gaps (Eg) of the $Zn_{1-x}Mg_xO$ nanoparticles were changed from 3.19 to 3.31 eV by increasing the incorporation of Mg^{2+} ion concentration in the $(Zn_{1-x}Mg_xO)$ nanoparticles. In other words, as the Mg^{2+} content increases, the band gap energy of the $Zn_{1-x}Mg_xO$ nanoparticles is widened. The increase in the value of the band gap energy is due to that the band gap energy of the MgO added to the structure is larger than the band gap energy of ZnO [36]. In addition, this increase can be imputed to the Burstein - Moss effect, the optical band gap increases because the substitution of Mg^{2+} ion into ZnO lattice leads to the generation of oxygen vacancies for charge compensation and thus modifies the electron density in the conduction band of ZnO [15]. Increasing impurities increases the concentration of charged particles, which partially fills the conduction band, making low level transitions almost impossible because they are filled with carriers (electrons), and thus transitions are only possible for high energy particles or photons[37]. The variation of optical band gap with Mg content of the $Zn_{1-x}Mg_xO$ nanoparticles are illustrated in Figure (10). It is observed that the energy band gap slightly increases with increasing Mgcontent.
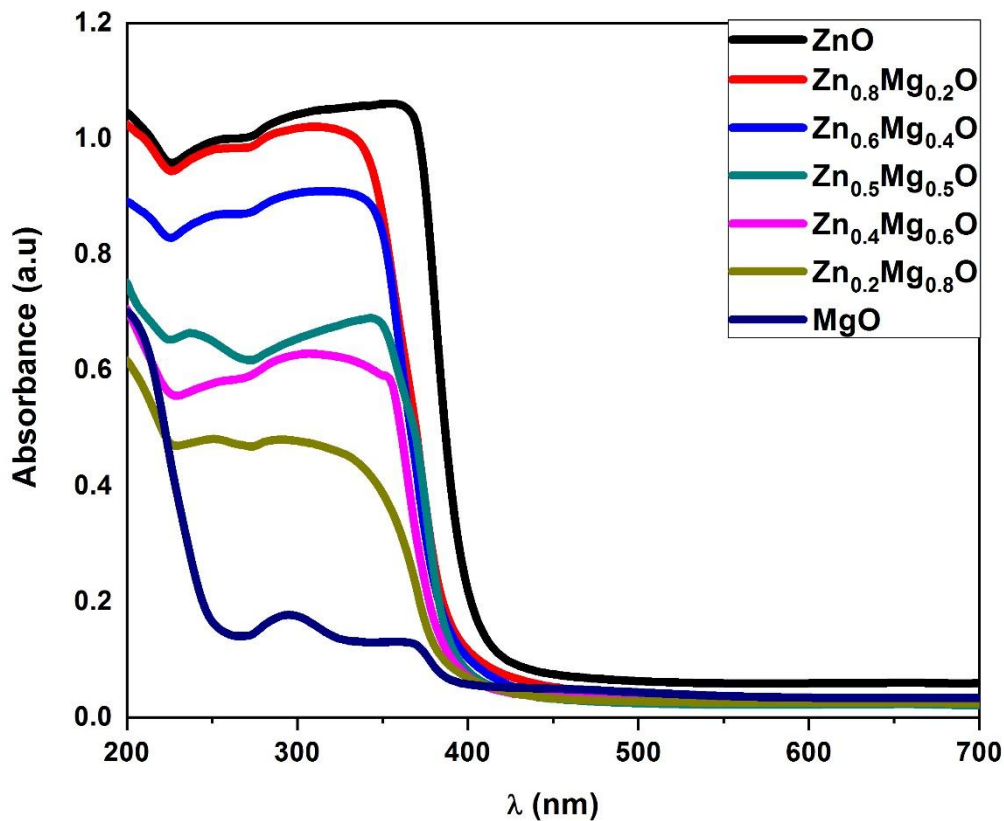

Fig 7. The Absorption spectra of $Zn_{1-x}Mg_xO$ nanoparticles.
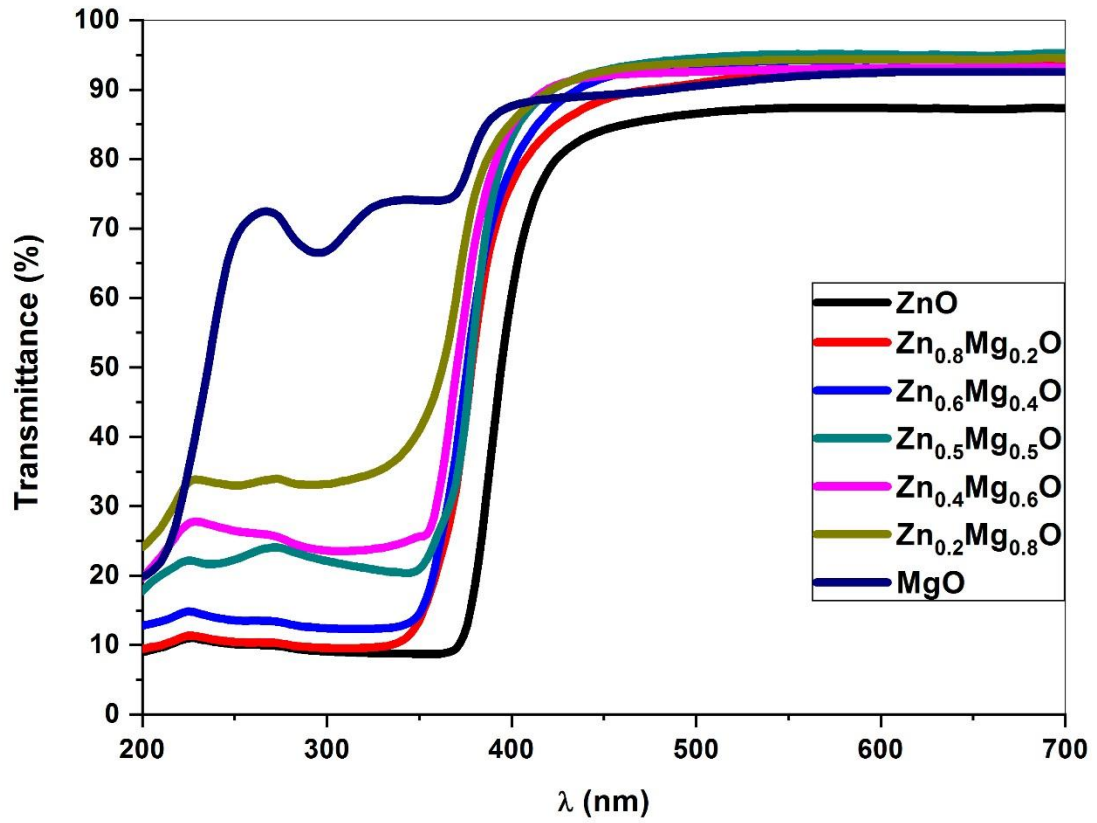
_____

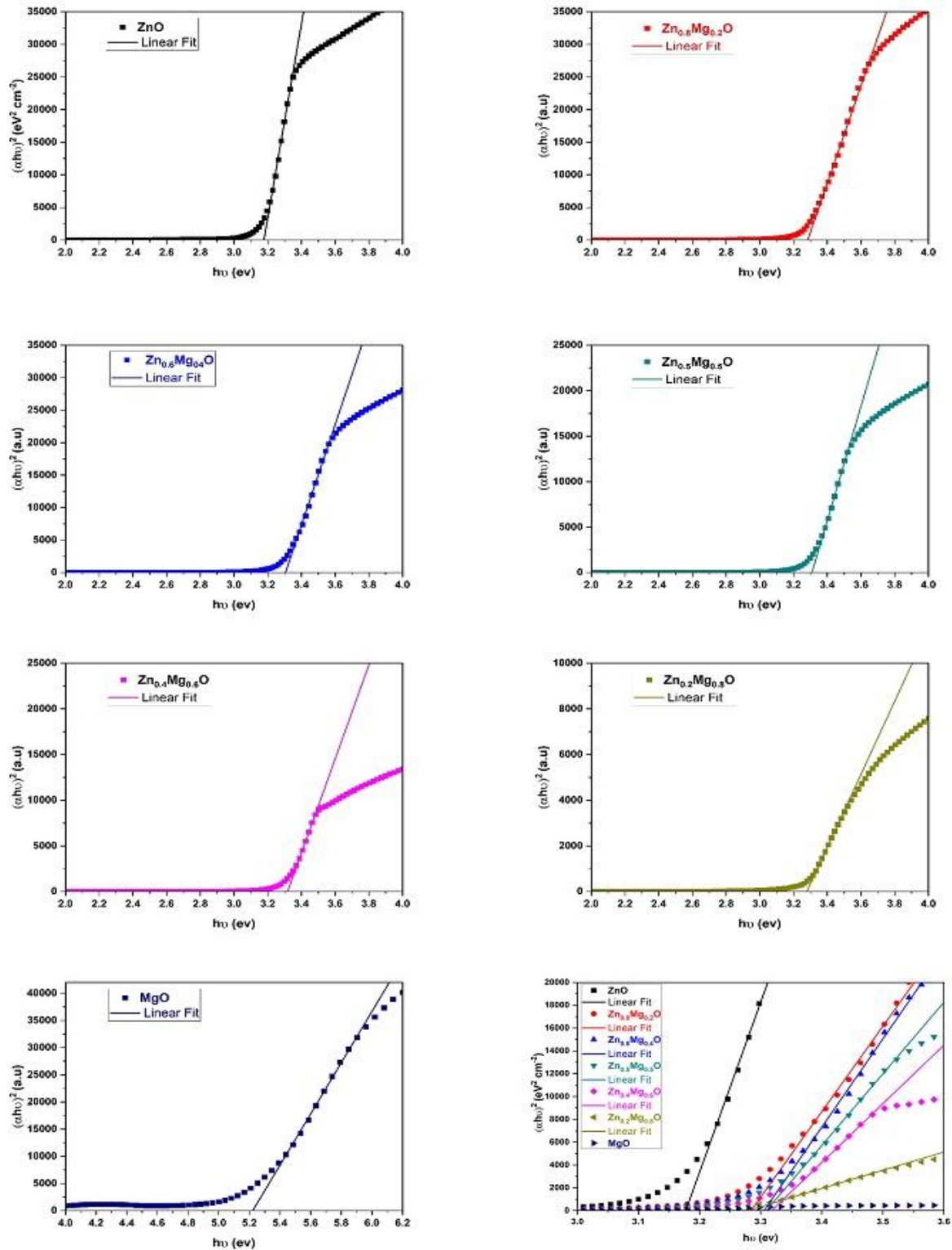**Fig. 8. The transmittance spectra of the $Zn_{1-x}Mg_xO$ nanocomposites.**

_____

Fig. 9. Tauc plots of $(\alpha h\upsilon)^2$ versus $h\upsilon$ to determine the optical bandgap of the $Zn_{1-x}Mg_xO$ nanocomposites.
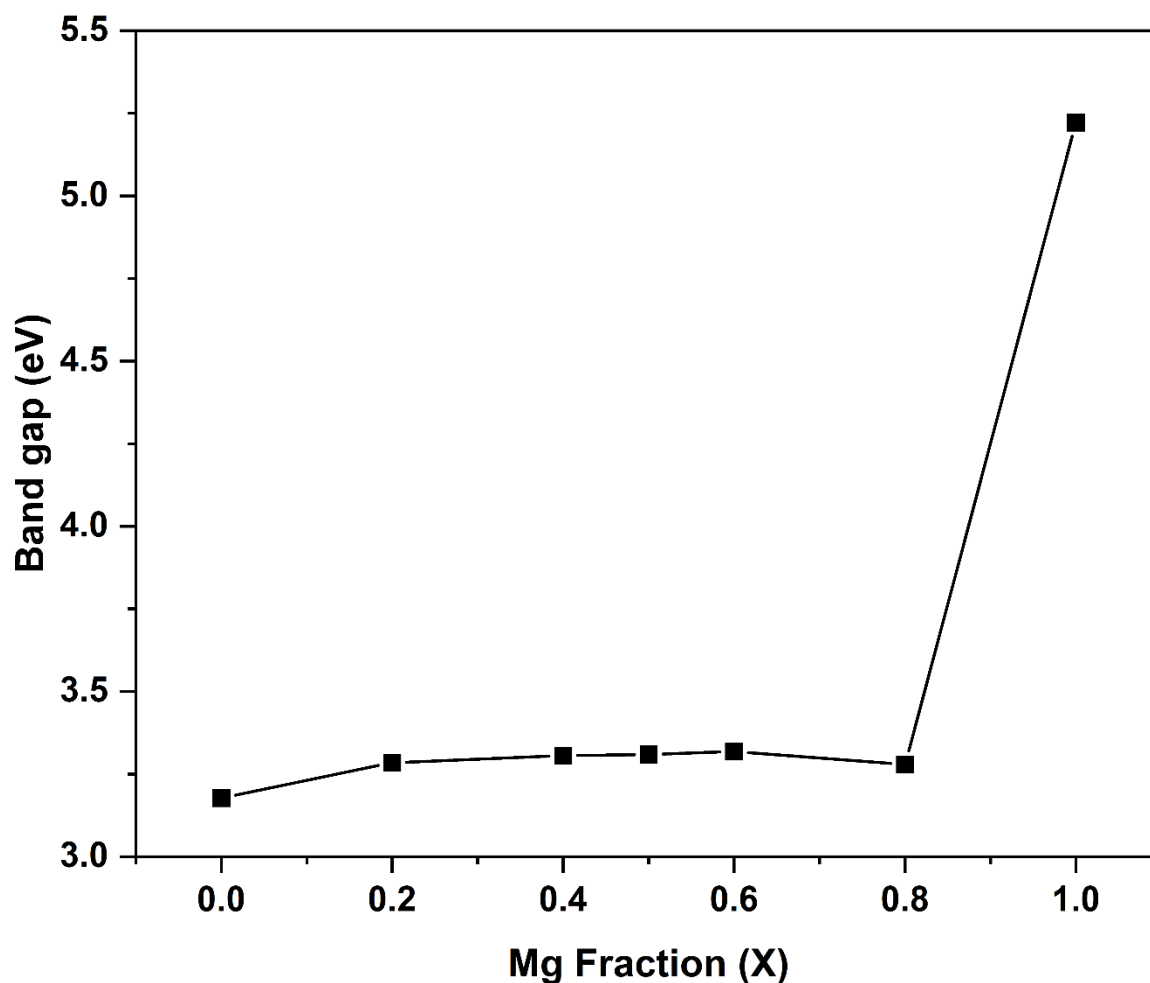
_____

Fig. 10. Variation of optical bandgap of the $Zn_{1-x}Mg_xO$ nanocompositeswith Mg fraction (x).

Photoluminescence spectroscopy of the $Zn_{1-x}Mg_xO$ nanoparticles

Room temperature PL spectra of the pure and $Zn_{1-x}Mg_xO$ nanocomposites excited at 320 nm wavelength are shown in Figure (11). Two distinguishable emissions were observed for all the samples, a near band-edge (UV) emission located within the 360 nm and a broad deep level emission in the visible region situated between 500 and 550 nm.

The strong UV emission around 360 nm is attributed by the radiative exciton recombination (exciton emission) between conduction band and valance band. Figure (11) show that the UV band of $Zn_{1-x}Mg_xO$ nanocomposites which is effectively enhanced with the increasing of Mg content. The UV intensity increase as Mg content increase from x=0 to x=0.4, and then decrease at x=0.5 and above. In comparison to the visible emission band, the UV band has a higher intensity. So, the formation of $Zn_{1-x}Mg_xO$ nanocomposites leads to the enhancement of UV emission.As a result of the presence of Mg in interstitial position, which forms a shallow donor state and gives an electron to the hole in zinc vacancies[38]. Consequently, the improvement of the UV PL intensity is related to the rise in the number of Mg interstitial defects which increases the recombination of Mg interstitial with zinc vacancies. The maximum UV intensity is obtained for the sample with x=0.4 of Mg concentration. Above this concentration, the UV emission is decrease indicating a decrease in Mg interstitial concentration.

The origin of the broad visible emission around 550 nm (green region) is attributed to the radiative recombination of photo-generated holes with electrons. It is mainly due to the structural defects in the $Zn_{1-x}Mg_xO$ nanocomposites such as vacancies and interstitials of zinc, magnesium, and oxygen which is surface anion vacancies [39]. The intensity of the visible emission decrease within the increase of Mg concentration. It is mean that the effect of increasing Mg content in the $Zn_{1-x}Mg_xO$ nanocomposites did not enhance the defect

emission and the oxygen vacancy concentration [40],this mean that $Zn_{1-x}Mg_xO$nanocomposites have defect concentrations less than the pure ZnO nanoparticles [7]. Previous literature reported that higher Mg content doping reduces the intensity of visible emission because of the recombination of photogenerated electrons and holes is being prevented by higher doping concentrations inside the ZnO NPs[41].
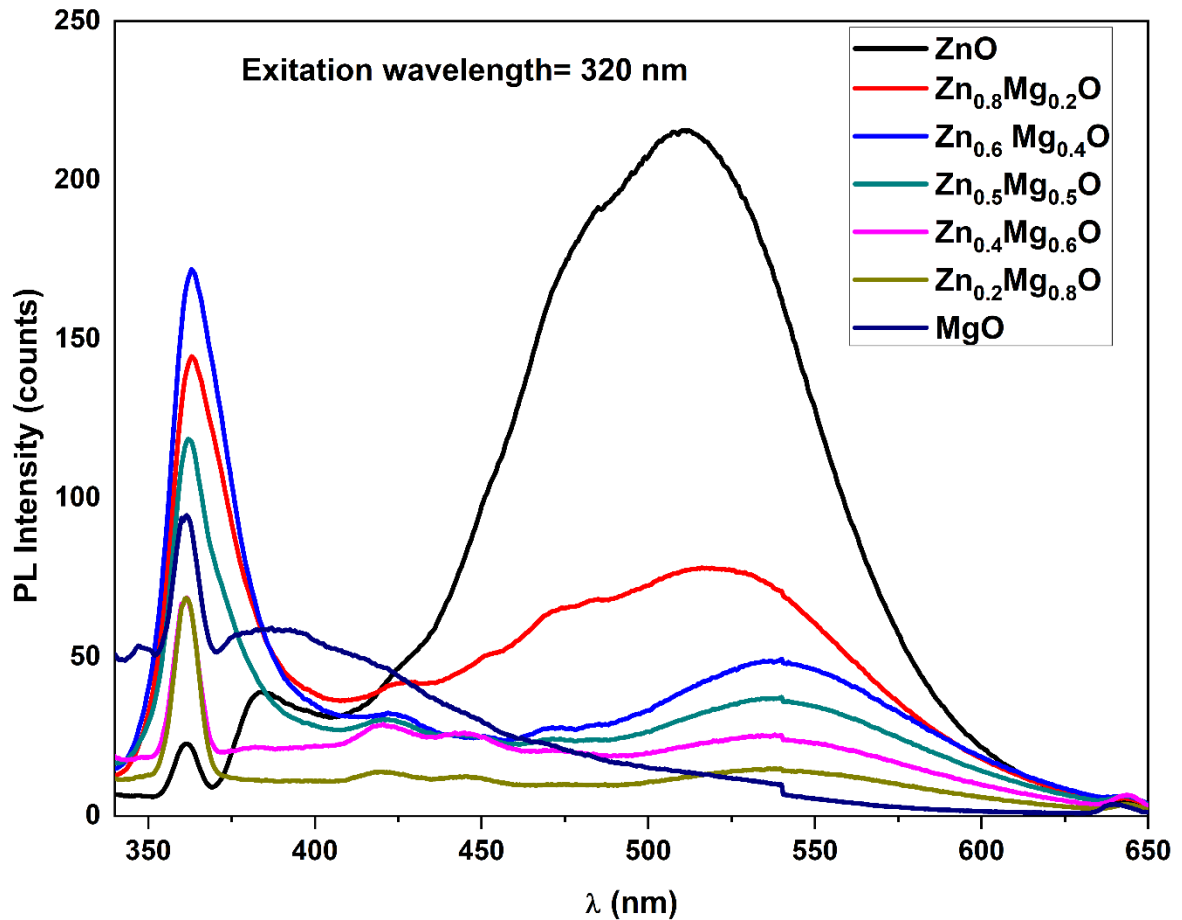

Fig. 11. Photoluminescence spectrum of $Zn_{1-x}Mg_xO$ nanocomposites.

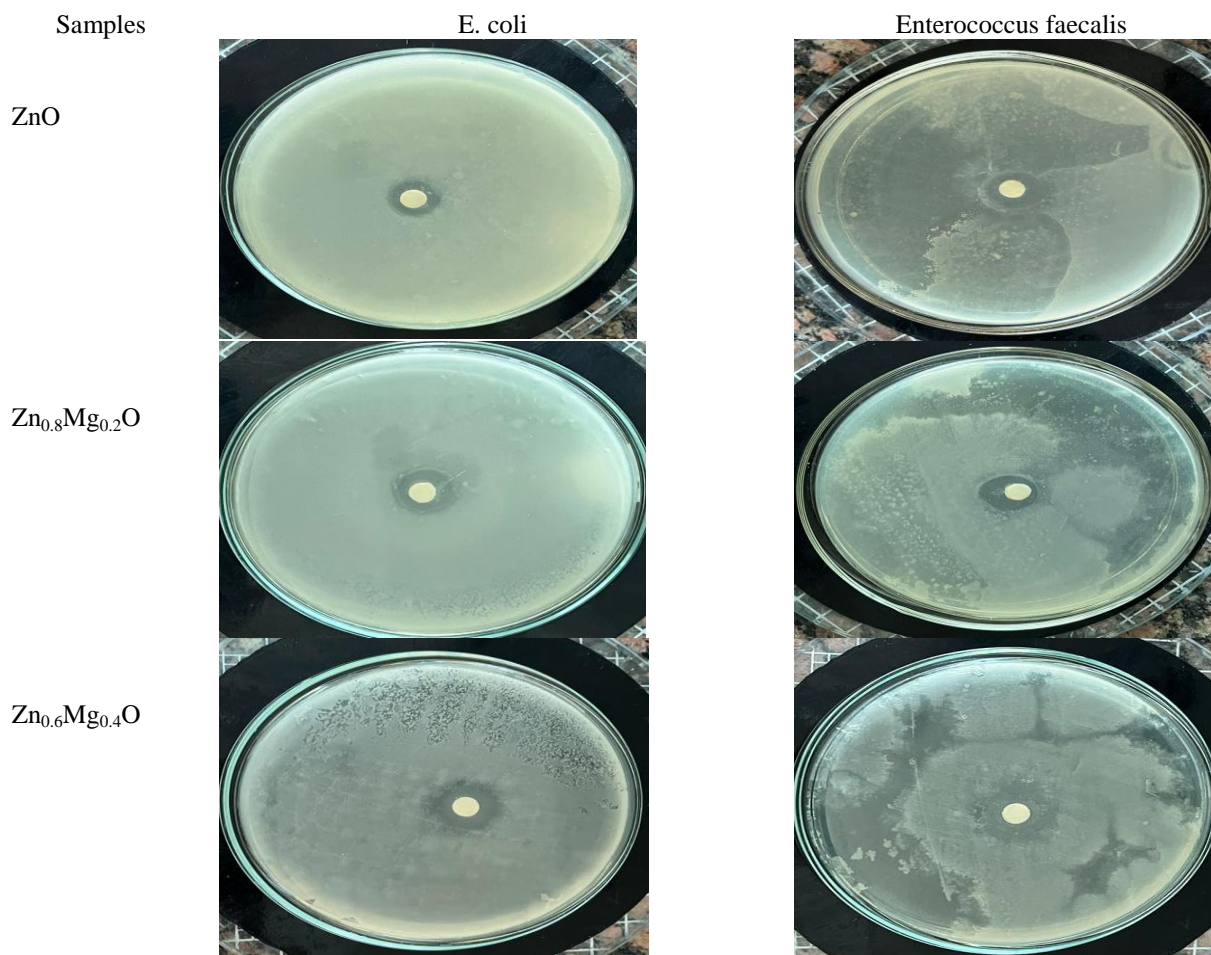*Antibacterial activity of $Zn_{1-x}Mg_xO$ nanocomposites*

The current study tested the ability of pure ZnO NPs, pure MgO NPs, and $Zn_{1-x}Mg_xO$ nanocomposites as potential antimicrobial agents against gram-negative (E. coli) and gram-positive bacteria (Enterococcus faecalis) using the disc diffusion method. The results clearly indicate that the ZnO and MgO nanoparticles inhibit the growth of both gram-negative and positive bacteria. It is found that the antibacterial activity of Gram-positive bacteria higher than Gram-negative bacteria due to the negatively charged radicals that readily adhere to the cell wall of Gram-positive bacteria and thus kill the bacteria [42]. The maximum antibacterial activity of ZnO nanoparticles was against (Enterococcus faecalis). This is due to the well-established attachment of ZnO molecules to the outer cell wall membrane of bacteria. Then, the ZnO molecules start to release oxygen species into the bacteria in the medium, stopping the cell from growing, causing the cell to deform and leak, eventually killing the cell[42].

The displayed photos in Figure (12) illustrate the formation of the inhibition zone of $Zn_{1-x}Mg_xO$ nanocomposites for (E. coli) Gram-negative and (Enterococcus faecalis) Gram-positive bacteria, the results show the ability of $Zn_{1-x}Mg_xO$ nanocomposites as a potential antimicrobial agent. The antibacterial activities of $Zn_{1-x}Mg_xO$ nanocomposite with different Mg ratios are given in Table (2). It was observed that the inhibition zone is affected by the increase in Mg concentration. The inhibition zoon of $Zn_{1-x}Mg_xO$ nanocomposites was found to increase as the mg ratio increase up to 0.4. After that, as the Mg ratio increase over 0.5 the antibacterial activitydecrease. $Zn_{1-x}Mg_xO$ nanocomposites showed better anti-microbial activity in comparison to pure ZnO and MgO NPs [43], especially for the samples with Mg ratio of x=0.2 and 0.4, where the inhibition zoon was enhanced from 12 to 15 mm in case of the gram-negative bacteria. The pure ZnO NPs have higher antibacterial

..
activity against the gram-positive bacteria (14 mm), but this value is slightly affected by increasing mg ratio. However, when the mg ratio become 0.5 and above the inhibition zoon decrease to (12 mm). It is mean that the $Zn_{1-x}Mg_xO$ nanocomposites with Zn concentration higher than Mg concentration have higher antibacterial activity, the increasing the Mg above x=0.5 leads to a decrease in antimicrobial activity.

The effect of Mg doping in ZnO nanoparticles might be attributed to the change in their band gap values. The optical bandgap widens because the substitution of Mgion into ZnO lattice generates oxygen vacancies for charge compensation,altering the electron density in the conduction band of ZnO. The growth inhibition capacity decreased with increasing dopant concentration, it can be attributed to the generation of singlet oxygen species [44].

The observed differences in the ability of oxide materials prepared with different amounts of Mg to generate singlet oxygen and antibacterial activities were related to differences in their structure and morphology. In the case of $Zn_{0.8}Mg_{0.2}O$ and $Zn_{0.6}Mg_{0.4}O$ nanocomposites, it is possible to suggest that the significant reduction in ZnO crystal size and the more dispersed morphology of these materials are the primary factors that contributed to their high antibacterial properties and capacity for singlet oxygen photogeneration[45]. It was found that $Zn_{0.8}Mg_{0.2}O$ and Zn0.6Mg0.4O nanocomposites showed better antibacterial activity in both bacterial cases.This was most likely caused by the increased surface-to-volume ratio of small particles, which have a greater ability to penetrate cell membranes and kill bacteria, where it was discovered that small particles have more antibacterial activity than large particles or amorphous particles in general[46].

Samples	E. coli	Enterococcus faecalis
ZnO		
$Zn_{0.8}Mg_{0.2}O$		
$Zn_{0.6}Mg_{0.4}O$		

_____

Zn$_{0.5}$Mg$_{0.5}$O

Zn$_{0.4}$Mg$_{0.6}$O

Zn$_{0.2}$Mg$_{0.8}$O

MgO
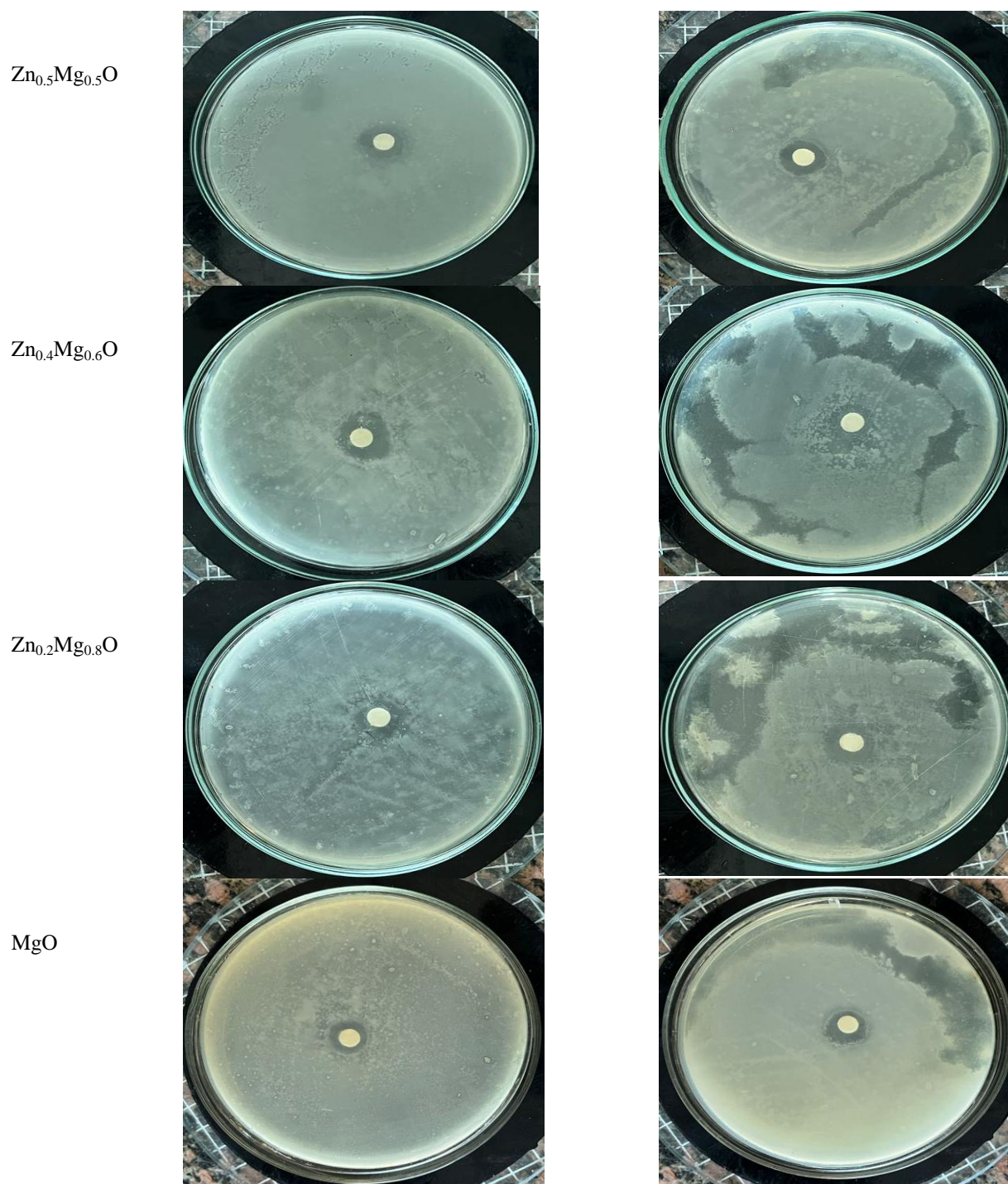
Fig. 12. Images illustrate the formation of the antibacterial inhibition zoon of the (Zn$_{1-x}$Mg$_x$O) nanoparticles.

..

TABLE 2. Effect of ($Zn_{1-x}Mg_xO$) nanocomposites on bacterial growth.

Sample	Diameter of inhibition zoon (mm)	
	Gram negative E. coli	Gram positive Enterococcus-faecalis
ZnO	12 ± 0.5	14 ± 0.5
$Zn_{0.8}Mg_{0.2}O$	14 ± 0.6	15 ± 0.4
$Zn_{0.6}Mg_{0.4}O$	15 ± 0.7	15 ± 0.5
$Zn_{0.5}Mg_{0.5}O$	14 ± 0.5	13 ± 0.7
$Zn_{0.4}Mg_{0.6}O$	12 ± 0.4	12 ± 0.3
$Zn_{0.2}Mg_{0.8}O$	13 ± 0.3	13 ± 0.5
MgO	13 ± 0.7	13 ± 0.3
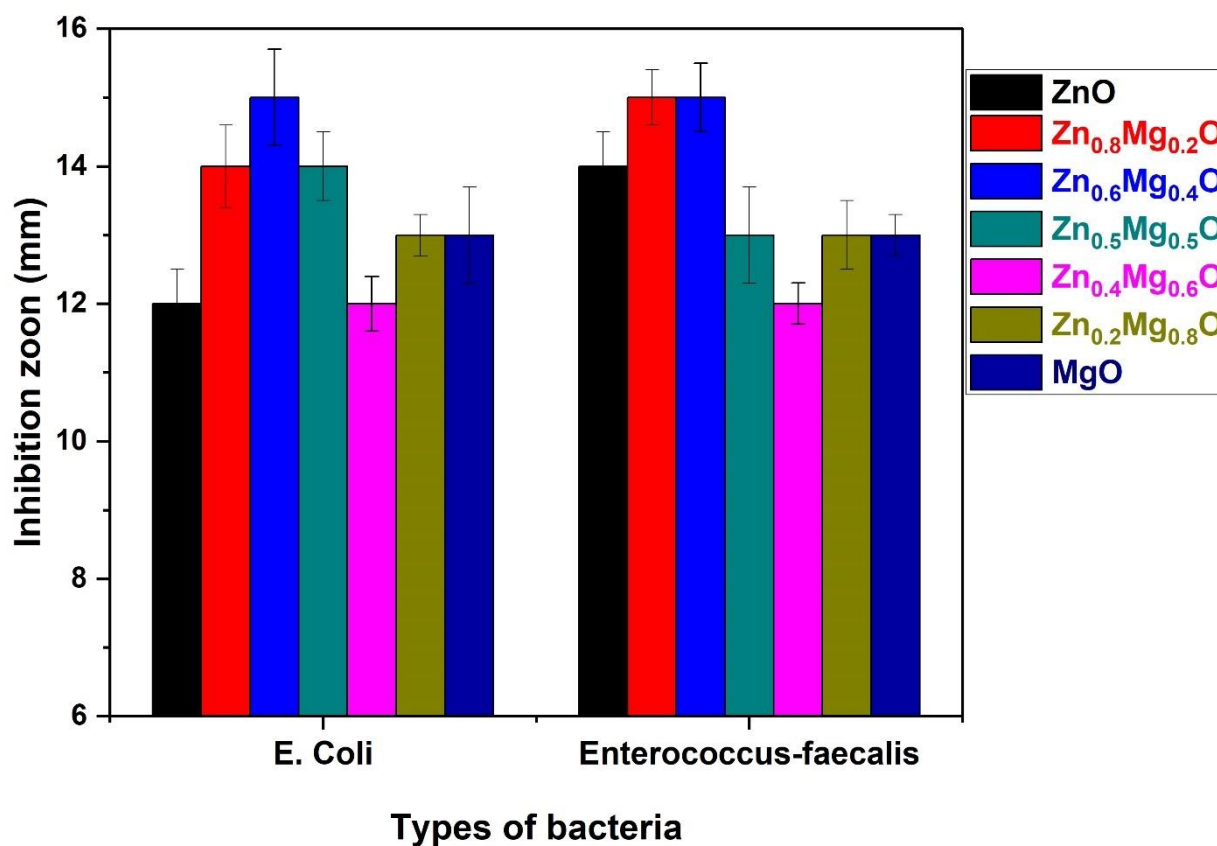
Fig, 13. The variation of antibacterial inhibition zoon of the ($Zn_{1-x}Mg_xO$) Nanocomposites with the Mg ratio.

_____

_____

Conclusions

The present work reported the structural, optical properties, and antibacterial activity of $Zn_{1-x}Mg_xO$ nanocomposites prepared through sol–gel method followed by the heat treatment at 550 °C. The FTIR expressed that the Zn-O and Mg-O bonds were present in the ZnO-MgO nanocomposites. TEM images confirmed that the existence of irregular, spherical and hexagonal shapes in nanoscale. XRD patterns of the samples proved the formation of nanocrystalline $Zn_{1-x}Mg_xO$ nanocomposites. XRD analysis showed that ZnO and MgO prefer to form separated phases with increase of Mg concentration in the $Zn_{1-x}Mg_xO$ nanocomposites. The UV–vis spectroscopy results showed that the band gap is slightly increase with increasing of Mg concentration. The PL spectra indicated that the UV emission intensity enhanced with increase of Mg concentration and there is a critical concentration beyond which there is no rise in the UV intensity. It was also found that the intensity of the visible emission depends on the concentration of Mg in $Zn_{1-x}Mg_xO$ nanocomposites. The $Zn_{1-x}Mg_xO$ nanocomposites showed a good antibacterial activity against E. coli and Enterococcus-faecalis compared to pure MgO and ZnO nanoparticles alone. The antibacterial activity of $Zn_{0.6}Mg_{0.4}O$ nanocomposites was higher than that of pure ZnO and MgONPs. The result concluded that $Zn_{1-x}Mg_xO$ nanocomposites have significant potential for antibacterial applications. The findings suggest that the particle size and morphology play vital role in their antibacterial activity.

References

[1]   M. P. Nikolova and M. S. Chavali, "Metal Oxide Nanoparticles as Biomedical Materials," *Biomimetics*, vol. 5, no. 2, p. 27, Jun. 2020, doi: 10.3390/biomimetics5020027.

[2]   M. S. Chavali and M. P. Nikolova, "Metal oxide nanoparticles and their applications in nanotechnology," *SN Appl. Sci.*, vol. 1, no. 6, p. 607, Jun. 2019, doi: 10.1007/s42452-019-0592-3.

[3]   S. Das and V. C. Srivasatava, "Synthesis and Characterization of ZnO–MgO Nanocomposite by Co-precipitation Method," *Smart Sci.*, vol. 4, no. 4, pp. 190–195, Oct. 2016, doi: 10.1080/23080477.2016.1260425.

[4]   S. Faisal, S. Naqvi, M. Ali, and L. Lin, "Comparative study of multifunctional properties of synthesised ZnO and MgO NPs for textiles applications," *Pigment Resin Technol.*, vol. 51, no. 3, pp. 301–308, 2022, doi: 10.1108/prt-02-2021-0017.

[5]   I. O. P. C. Series and M. Science, "Synthesis , Characterization and antibacterial activity of Magnesium Oxide (MgO) nanoparticles . Synthesis , Characterization and antibacterial activity of Magnesium Oxide (MgO) nanoparticles .," 2019, doi: 10.1088/1757-899X/577/1/012051.

[6]   J. Pachiyappan, N. Gnanasundaram, and G. L. Rao, "Preparation and characterization of ZnO, MgO and ZnO–MgO hybrid nanomaterials using green chemistry approach," *Results Mater.*, vol. 7, no. May, p. 100104, 2020, doi: 10.1016/j.rinma.2020.100104.

[7]   S. Klubnuan, P. Amornpitoksuk, and S. Suwanboon, "Structural, optical and photocatalytic properties of MgO/ZnO nanocomposites prepared by a hydrothermal method," *Mater. Sci. Semicond. Process.*, vol. 39, pp. 515–520, 2015, doi: 10.1016/j.mssp.2015.05.049.

[8]   A. E. Kandjani, M. F. Tabriz, and B. Pourabbas, "Sonochemical synthesis of ZnO nanoparticles: The effect of temperature and sonication power," *Mater. Res. Bull.*, vol. 43, no. 3, pp. 645–654, Mar. 2008, doi: 10.1016/j.materresbull.2007.04.005.

[9]   D. Chhikara, K. M. K. Srivatsa, and S. K. Muthusamy, "On the synthesis and characterization of ZnO/MgO nanocomposite by thermal evaporation technique," *Solid State Sci.*, vol. 37, pp. 108–113, Nov. 2014, doi: 10.1016/j.solidstatesciences.2014.09.002.

[10]   A. N. Baranov, O. O. Kurakevych, V. A. Tafeenko, P. S. Sokolov, G. N. Panin, and V. L. Solozhenko, "High-pressure synthesis and luminescent properties of cubic ZnO/MgO nanocomposites," *J. Appl. Phys.*, vol. 107, no. 7, p. 073519, Apr. 2010, doi: 10.1063/1.3359661.

[11]   C. R. Indulal, R. Biju, D. Nand, and R. Raveendran, "Optical and antibacterial studies of zinc magnesium oxide nanocomposite," *Orient. J. Chem.*, vol. 33, no. 3, pp. 1545–1549, 2017, doi: 10.13005/ojc/330359.

[12]   M. D. Jaafer, A. H. Omran Al-khayatt, and S. M. Saleh, "Structural, Surface Topography and Optical Characterization of Nanocrystalline Mg x Zn 1-x O Thin Films Grown by Modified Chemical Bath Deposition (SILAR) Method," *J. Phys. Conf. Ser.*, vol. 1234, no. 1, p. 012001, Jul. 2019, doi: 10.1088/1742-6596/1234/1/012001.

_____

..

[13]   A. J. Ahamed, P. V. Kumar, and M. Karthikeyan, "Synthesis, Structural and Antibacterial Properties of Mg Doped ZnO Nanoparticles," *J. Environ. Nanotechnol.*, vol. 5, no. 2, pp. 11–16, 2016, doi: 10.13074/jent.2016.06.162189.

[14]   G. Kasi, K. Viswanathan, K. Sadeghi, and J. Seo, "Optical, thermal, and structural properties of polyurethane in Mg-doped zinc oxide nanoparticles for antibacterial activity," *Prog. Org. Coatings*, vol. 133, no. February, pp. 309–315, 2019, doi: 10.1016/j.porgcoat.2019.04.066.

[15]   G. Kasi and J. Seo, "Influence of Mg doping on the structural, morphological, optical, thermal, and visible-light responsive antibacterial properties of ZnO nanoparticles synthesized via co-precipitation," *Mater. Sci. Eng. C*, vol. 98, no. March 2018, pp. 717–725, 2019, doi: 10.1016/j.msec.2019.01.035.

[16]   A. K. Worku *et al.*, "Structural and thermal properties of pure and chromium doped zinc oxide nanoparticles," *SN Appl. Sci.*, vol. 3, no. 7, 2021, doi: 10.1007/s42452-021-04682-6.

[17]   S. Sagadevan, S. Vennila, J. A. Lett, A. R. Marlinda, N. A. B. Hamizi, and M. R. Johan, "Tailoring the structural, morphological, optical, thermal and dielectric characteristics of ZnO nanoparticles using starch as a capping agent," *Results Phys.*, vol. 15, no. July, 2019, doi: 10.1016/j.rinp.2019.102543.

[18]   A. Ansari, A. Ali, M. Asif, and Shamsuzzaman, "Microwave-assisted MgO NP catalyzed one-pot multicomponent synthesis of polysubstituted steroidal pyridines," *New J. Chem.*, vol. 42, no. 1, pp. 184–197, 2018, doi: 10.1039/c7nj03742b.

[19]   G. Lu, I. Lieberwirth, and G. Wegner, "A General Polymer-Based Process To Prepare Mixed Metal Oxides: The Case of Zn 1- x Mg x O Nanoparticles," *J. Am. Chem. Soc.*, vol. 128, no. 48, pp. 15445–15450, Dec. 2006, doi: 10.1021/ja0638096.

[20]   V. Sukauskas, "Characterization of MgZnO epitaxial layers with high Mg concentration," KTH Royal Institute of Technology and Vilnius University, 2011.

[21]   P. Bindu and S. Thomas, "Estimation of lattice strain in ZnO nanoparticles: X-ray peak profile analysis," *J. Theor. Appl. Phys.*, vol. 8, no. 4, pp. 123–134, Dec. 2014, doi: 10.1007/s40094-014-0141-9.

[22]   S. El-Nahas, M. S. A. El-sadek, H. M. Salman, and M. M. Elkady, "Controlled morphological and physical properties of ZnO nanostructures synthesized by domestic microwave route," *Mater. Chem. Phys.*, vol. 258, no. July 2020, p. 123885, 2021, doi: 10.1016/j.matchemphys.2020.123885.

[23]   M. Bodke, U. Gawai, A. Patil, and B. Dole, "Estimation of accurate size, lattice strain using Williamson-Hall models, SSP and TEM of Al doped ZnO nanocrystals," *Matériaux Tech.*, vol. 106, no. 6, p. 602, Feb. 2018, doi: 10.1051/mattech/2018055.

[24]   K. Ravichandran, S. Snega, N. Jabena Begum, L. Rene Christena, S. Dheivamalar, and K. Swaminathan, "Effect of Mg doping level on the antibacterial activity of (Mg + F)-doped ZnO nanopowders synthesized using a soft chemical route," *Philos. Mag.*, vol. 94, no. 22, pp. 2541–2550, 2014, doi: 10.1080/14786435.2014.921349.

[25]   S. Suwanboon, P. Amornpitoksuk, and A. Sukolrat, "Dependence of optical properties on doping metal, crystallite size and defect concentration of M-doped ZnO nanopowders (M = Al, Mg, Ti)," *Ceram. Int.*, vol. 37, no. 4, pp. 1359–1365, 2011, doi: 10.1016/j.ceramint.2010.12.010.

[26]   K. Ravichandran *et al.*, "Influence of a novel triple doping (Ag+Mn+F) on the magnetic and antibacterial properties of ZnO nanopowders," *Ceram. Int.*, vol. 42, no. 2, pp. 2349–2356, 2016, doi: 10.1016/j.ceramint.2015.10.031.

[27]   A. N. Baranov, O. O. Kapitanova, G. N. Panin, and T. V. Kang, "ZnO/MgO nanocomposites generated from alcoholic solutions," *Russ. J. Inorg. Chem.*, vol. 53, no. 9, pp. 1366–1370, 2008, doi: 10.1134/S0036023608090040.

[28]   M. S. Abd El-Sadek, H. S. Wasly, and K. M. Batoo, "X-ray peak profile analysis and optical properties of CdS nanoparticles synthesized via the hydrothermal method," *Appl. Phys. A*, vol. 125, no. 4, p. 283, Apr. 2019, doi: 10.1007/s00339-019-2576-y.

[29]   J. Markmann, V. Yamakov, and J. Weissmüller, "Validating grain size analysis from X-ray line broadening: A virtual experiment," *Scr. Mater.*, vol. 59, no. 1, pp. 15–18, Jul. 2008, doi: 10.1016/j.scriptamat.2008.02.056.

[30]   J. Madhavi, "Comparison of average crystallite size by X-ray peak broadening and Williamson–Hall and size–strain plots for VO2+ doped ZnS/CdS composite nanopowder," *SN Appl. Sci.*, vol. 1, no. 11, p. 1509, Nov. 2019, doi: 10.1007/s42452-019-1291-9.

[31]   H. Hussain *et al.*, "Investigation of magnesium addition in ZnO matrix using group II heptahydrate," *Mater. Res. Express*, vol. 8, no. 4, 2021, doi: 10.1088/2053-1591/abf1a0.

[32]   R. A.-F. Ibrahim, "Study the Effect of MgO on the Photocatalysis of ZnO Thin Layers," Al- Azhar University, 2011.

[33]   A. Attaf *et al.*, "The effect of the solution flow rate on the properties of zinc oxide (ZnO) thin films deposited by ultrasonic spray," 2015, p. 020015, doi: 10.1063/1.4914206.

[34]   L. Dimesso, M. Wussler, T. Mayer, E. Mankel, and W. Jaegermann, "Inorganic alkali lead iodide

_____

_____

semiconducting APbI3 (A = Li, Na, K, Cs) and NH4PbI3 films prepared from solution: Structure, morphology, and electronic structure," *AIMS Mater. Sci.*, vol. 3, no. 3, pp. 737–755, 2016, doi: 10.3934/matersci.2016.3.737.

[35]   J. Tauc, "Optical properties and electronic structure of amorphous Ge and Si," *Mater. Res. Bull.*, vol. 3, no. 1, pp. 37–46, Jan. 1968, doi: 10.1016/0025-5408(68)90023-8.

[36]   S. Temel, M. Nebi, and D. Peker, "Optical band gap engineering of (MgO)x(ZnO)1-x films deposited by sol-gel spin coating," *Optoelectron. Adv. Mater. Rapid Commun.*, vol. 12, no. 1–2, pp. 76–79, 2018.

[37]   P. Panchal *et al.*, "Phytoextract mediated ZnO/MgO nanocomposites for photocatalytic and antibacterial activities," *J. Photochem. Photobiol. A Chem.*, vol. 385, no. June, p. 112049, 2019, doi: 10.1016/j.jphotochem.2019.112049.

[38]   S. Chawla, K. Jayanthi, H. Chander, D. Haranath, S. K. Halder, and M. Kar, "Synthesis and optical properties of ZnO/MgO nanocomposite," *J. Alloys Compd.*, vol. 459, no. 1–2, pp. 457–460, 2008, doi: 10.1016/j.jallcom.2007.04.303.

[39]   C. Abed, M. Ben Ali, A. Addad, and H. Elhouichet, "Growth, structural and optical properties of ZnO-ZnMgO-MgO nanocomposites and their photocatalytic activity under sunlight irradiation," *Mater. Res. Bull.*, vol. 110, no. September 2018, pp. 230–238, 2019, doi: 10.1016/j.materresbull.2018.10.041.

[40]   G. Gupta, S. Verma, R. Nagarajan, and S. Rath, "Microstructural and bandgap investigations of wurtzite-phase ZnMgO nanopowders synthesized by ball-milling," *Phys. B Condens. Matter*, vol. 604, no. October 2020, p. 412735, 2021, doi: 10.1016/j.physb.2020.412735.

[41]   K. Pradeev raj *et al.*, "Influence of Mg Doping on ZnO Nanoparticles for Enhanced Photocatalytic Evaluation and Antibacterial Analysis," *Nanoscale Res. Lett.*, vol. 13, 2018, doi: 10.1186/s11671-018-2643-x.

[42]   R. Sakthivel, A. Shankar Ganesh, A. Geetha, B. Anandh, R. Kannusamy, and K. Tamilselvan, "Effect of Post Annealing on Antibacterial Activity of Zno thin films Prepared by Modified Silar Technique," *Orient. J. Chem.*, vol. 33, no. 1, pp. 355–362, Feb. 2017, doi: 10.13005/ojc/330142.

[43]   A. Nigam, S. Saini, A. K. Rai, and S. J. Pawar, "Structural, optical, cytotoxicity, and antimicrobial properties of MgO, ZnO and MgO/ZnO nanocomposite for biomedical applications," *Ceram. Int.*, vol. 47, no. 14, pp. 19515–19525, 2021, doi: 10.1016/j.ceramint.2021.03.289.

[44]   M. Perez-Altamar, H. Marrero, M. Martinez Julca, and O. Perales Perez, "Study of bactericidal properties of Mg-doped ZnO nanoparticles," *Mater. Res. Soc. Symp. Proc.*, vol. 1804, pp. 31–36, 2015, doi: 10.1557/opl.2015.543.

[45]   A. A. Shelemanov *et al.*, "Enhanced singlet oxygen photogeneration by bactericidal ZnO–MgO–Ag nanocomposites," *Mater. Chem. Phys.*, vol. 276, no. September 2021, p. 125204, 2022, doi: 10.1016/j.matchemphys.2021.125204.

[46]   P. Panchal *et al.*, "Phytoextract mediated ZnO/MgO nanocomposites for photocatalytic and antibacterial activities," *J. Photochem. Photobiol. A Chem.*, vol. 385, no. July, p. 112049, 2019, doi: 10.1016/j.jphotochem.2019.112049.

_____